The Astrophysical Journal, 756:98 (7pp), 2012 September 1 doi:10.1088/0004-637X/756/1/98

FORMATION OF MOLECULAR OXYGEN AND OZONE ON AMORPHOUS SILICATES

Dapeng Jing[1], Jiao He[1], John Robert Brucato[2], Gianfranco Vidali[1], Lorenzo Tozzetti[2], and Antonio De Sio[3]
[1] Physics Department, Syracuse University, Syracuse, NY 13244, USA
[2] Osservatorio Astrofisico di Arcetri, INAF, I-50125 Florence, Italy
[3] Department of Physics and Astronomy, University of Florence, I-50125 Florence, Italy
Received 2012 March 14; accepted 2012 July 05; published 2012 August 20

ABSTRACT

Oxygen in the interstellar medium is seen in the gas phase, in ices (incorporated in H_2O, CO, and CO_2), and in grains such as $(Mg_xFe_{1-x})SiO_3$ or $(Mg_xFe_{1-x})_2SiO_4$, $0 < x < 1$. In this investigation, we study the diffusion of oxygen atoms and the formation of oxygen molecules and ozone on the surface of an amorphous silicate film. We find that ozone is formed at low temperature (<30 K), and molecular oxygen forms when the diffusion of oxygen atoms becomes significant, at around 60 K. This experiment, besides being the first determination of the diffusion energy barrier (1785 ± 35 K) for oxygen atoms on a silicate surface, suggests bare silicates as a possible storage place for oxygen atoms in low-A_v environments.

Key words: astrochemistry – dust, extinction – ISM: molecules – methods: laboratory – molecular processes

Online-only material: color figures

1. INTRODUCTION

Oxygen is the third most abundant element in space. Atomic oxygen is seen in diffuse clouds at 3×10^{-4} of H_2 (Ehrenfreund & van Dishoeck 1998; Meyer et al. 1998). Measurements of molecular oxygen in dense dark clouds with *SWAS* and *Odin* gave upper limits of 1×10^{-7} to 3×10^{-6} (Goldsmith et al. 2000; Liseau et al. 2010; Pagani et al. 2003). However, these values are much lower than that predicted by gas-phase models. Oxygen take-up in silicates cannot be responsible for the missing abundance in the gas phase because it is constrained by the abundance of Si, Fe, and Mg. The efficiency of O_2 adsorption on grains is also limited due to evaporation and cosmic-ray-induced desorption. However, oxygen can be locked in volatile molecules that make up ices covering dust grains in dense clouds (Hincelin et al. 2011). Ices in dense clouds are mainly composed of water molecules with significant fractions of CO_2, CO, CH_3OH, etc. (Ehrenfreund & Charnley 2000). The accepted explanation for the oxygen depletion is that in dark clouds oxygen adsorbed on grains is converted into water and CO_2 by either atomic addition processes or by the aid of cosmic rays (Bergin et al. 2000), such as:

$$O_2 + \text{c.r.} \rightarrow O + O \tag{1}$$

$$O + H \rightarrow OH, \ OH + H \rightarrow H_2O \tag{2}$$

$$O + O_2 \rightarrow O_3; \ O_3 + H \rightarrow O_2 + OH;$$
$$OH + H \rightarrow H_2O \text{ or } OH + H_2 \rightarrow H_2O + H \tag{3}$$

$$O + CO \rightarrow CO_2. \tag{4}$$

These processes have been studied in laboratories using CO molecules and thermal oxygen atoms (Raut & Baragiola 2011; Roser et al. 2001), superthermal oxygen atoms (Madzunkov et al. 2010), and thermal oxygen and hydrogen atoms (Jing et al. 2011). In Reactions (3), ozone, as an intermediate product, has not been found in the interstellar medium (ISM), probably because it is consumed by rapid reactions leading to the formation of water. This reaction scheme has been studied in experiments of interaction of D atoms on O_3 deposited on water ice (Mokrane et al. 2009; Romanzin et al. 2011). Ozone formation has also been studied in the laboratory using suprathermal oxygen atoms generated by energetic electrons or ions (Bennett & Kaiser 2005; Ennis et al. 2011; Sivaraman et al. 2007).

Modifications to the above theory have also been made by Bergin et al. (2003), Hollenbach et al. (2009), and Spaans & van Dishoeck (2001). It is believed that significant amounts of water and CO_2 are formed on grain surfaces at low temperature, as gas-phase reactions cannot account for the observed abundances. Whether water is CO_2 are formed by neutral atom addition or initiated by cosmic rays or UV, the diffusion of oxygen on surfaces is involved in elementary reaction steps. Oxygen mobility is also important in the formation of larger molecules. For example, oxygen reacts with CH_3 to form CH_3O, leading to the formation of methanol (Garrod & Pauly 2011).

In this contribution, we report the first measurement of the diffusion of thermal oxygen atoms on the surface of a dust grain analog, an amorphous silicate thin film. The diffusion of oxygen atoms leads to the formation of molecular oxygen and ozone. These measurements should help assess the relative efficiency of thermal versus suprathermal mobility of oxygen atoms in ozone formation. Furthermore, the study of the ozone channel in water formation relies on the formation of ozone via oxygen diffusion and reaction with O_2 molecules. This paper is organized as follows. The experimental methods are described in the next section. In Section 3, we present our mass spectrum results of O_2 and O_3 formation and rate equation simulation results revealing relevant energetic parameters. In Section 4, astrophysical implications of the results are presented. At the end, a brief summary is provided in Section 5.

2. EXPERIMENTAL

The experiments were conducted in an ultra-high-vacuum setup (see Figure 1) with a main chamber and two atomic/molecular beamlines. The main chamber is pumped by a turbomolecular pump, an ion pump, and a cryopump and has a base pressure of less than 2×10^{-10} Torr at room temperature. A triple-pass Hiden HAL/3F quadrupole mass spectrometer (QMS) is mounted on a rotary platform for temperature-programmed desorption (TPD) measurements

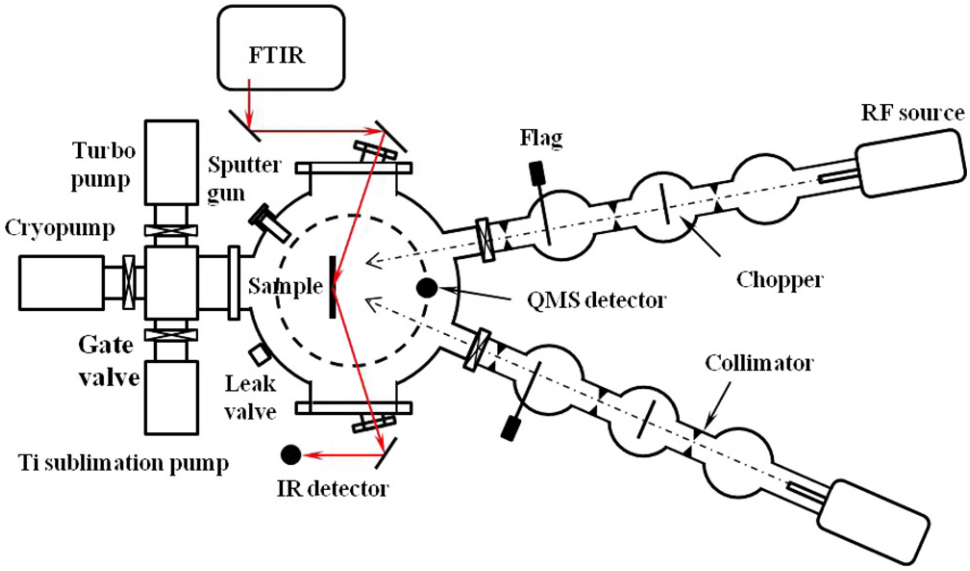

Figure 1. Top view of the experimental setup.
(A color version of this figure is available in the online journal.)

as well as beam flux and composition measurements. A Nicolet 6700 Fourier transform infrared spectrometer is configured to make reflection absorption infrared spectroscopy measurements. The sample used in this study is a 3 μm thick amorphous thin film of silicate deposited on a 0.5 inch diameter gold-coated copper disk. The film was prepared at the University of Florence by using a 9 kV electron beam impinging on a target consisting of MgO, FeO, and SiO_2 mixed to olivine $(MgFe)SiO_4$ stoichiometry. The sample is then mounted on a cold finger attached to a three-axis manipulator on a rotatable flange. Its temperature can be varied from 8 K to 500 K and is measured by a calibrated LakeShore silicon diode thermometer. The sample is cleaned by repeatedly heating to 400 K in vacuum during bakeout and prior to each experiment. The two beamlines each consist of three independently pumped chambers separated by collimators with a diameter of 2 mm. A laser is mounted on each beamline behind the gas source to align the two lines to produce an overlapping spot on the sample. The beams can be controlled by a flag in the third chamber and a mechanical chopper in the second chamber (see Figure 1). Radio frequency (RF) dissociation sources are attached to generate ^{16}O and ^{18}O atoms from their parent molecules. It is believed that the oxygen atoms generated by the RF sources are in their ground state ^3P, while the excited state ^1D is quenched by O_2 (Roser et al. 2001; Balucani et al. 2004). A final adjustment of the sample position is done so as to obtain the largest yield of $^{16}O^{18}O$ from ^{16}O and ^{18}O simultaneous exposure.

The QMS detector can be rotated to directly measure the beam flux and composition. A detailed description of the flux measurement method can be found elsewhere (Jing et al. 2011). When the RF sources are turned on, the ^{16}O beam dissociation efficiency is 16.0% $\pm$ 4.3% and that for the ^{18}O beam is 41.9% $\pm$ 5.2%. The measured ^{16}O flux is $(1.02 \pm 0.29) \times 10^{11}$ s^{-1}, $^{16}O_2$ flux is $(2.63 \pm 0.10) \times 10^{11}$ s^{-1}, ^{18}O flux is $(2.43 \pm 0.56) \times 10^{11}$ s^{-1}, and $^{18}O_2$ flux is $(1.64 \pm 0.12) \times 10^{11}$ s^{-1}. The error originates from day-to-day variations of the RF dissociation efficiencies. However, during a run, the dissociation rates are stable.

In a typical experiment, the sample is first heated to 400 K to desorb impurities while the sample holder is cooled with liquid helium to keep the background pressure below the 5×10^{-10} Torr range. For measurements, the sample is held at a temperature usually between 10 K and 60 K and is simultaneously exposed to $^{16}O/^{16}O_2$ and $^{18}O/^{18}O_2$ beams (exposure phase). After the desired exposure time, the beam flux is cut off and the sample is first cooled down to 15 K (if the exposure temperature is higher than 30 K) and heated up to 250 K to desorb surface species (TPD phase). The heating rate is about 1 K s^{-1}. The QMS detector placed in front of the sample detects the desorbed materials and a TPD trace is generated. The QMS is set to record simultaneously all the relevant masses of interest. However, this inevitably leads to a loss of signal/noise.

3. RESULTS AND DISCUSSION

3.1. Mass Spectrometry

In this subsection, we present in detail our experimental results based on mass analysis of molecules formed on the surface. First, we study molecular oxygen adsorption on and desorption from the silicate surface. The sample is exposed to a beam of $^{18}O_2$ molecules (RF off) at 20 K where the sticking coefficient of O_2 on silicate is close to unity as obtained from a sticking coefficient measurement using the well-established King & Wells adsorption–reflection method (King & Wells 1972). Desorption peaks from various exposures are shown in Figure 2(a). Stacking of the TPD traces shows that as coverage increases, the peak temperature first decreases and then increases (see Figure 2(b)). We interpret this behavior as follows. Below 10 minute exposure, the coverage is in sub-monolayer (ML) regime and the shift in the peak temperature is due to lateral interaction; perhaps clustering occurs. Beyond 10 minutes, O_2 coverage exceeds 1 ML and ice is building up. This interpretation is reinforced by the calculation of the O_2 coverage from the molecular beam flux value presented in Section 2. In sub-monolayer coverage, desorption follows first-order kinetics. Beyond a layer, desorption follows zeroth-order kinetics evidenced by coinciding leading edge and peak temperature shift to a higher value for higher coverage (Kolasinski 2008). This result of physisorbed O_2 is similar to what has been observed by Dohnalek et al. (2006) in

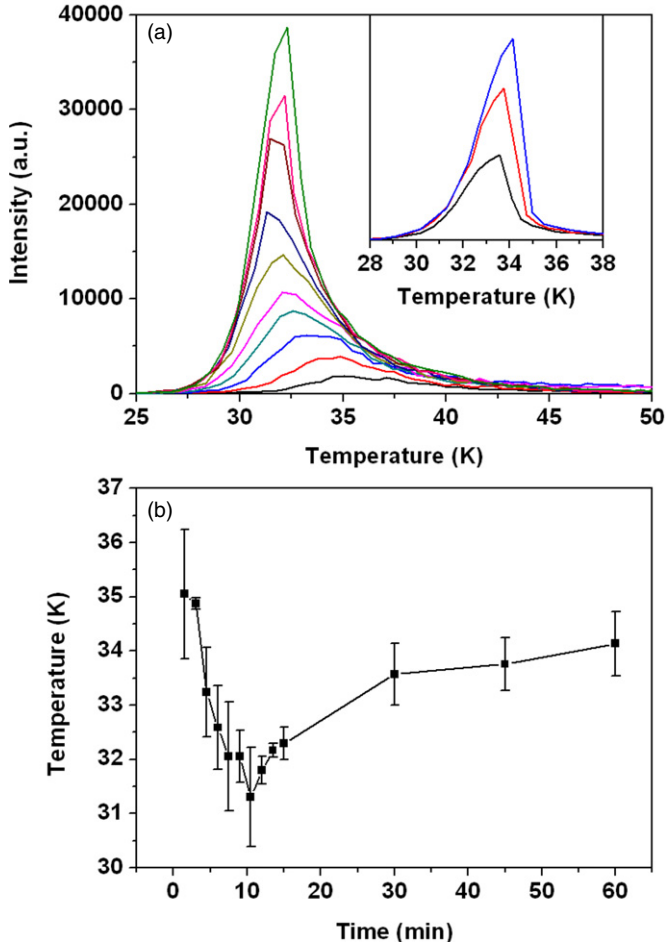

Figure 2. (a) Molecularly adsorbed oxygen desorption peaks after various exposure times at 20 K. From bottom to top, every 1.5 minutes from 1.5 minutes to 15 minutes. Inset from bottom to top: 30 minutes, 45 minutes, and 60 minutes. (b) Desorption peak temperature as a function of exposure time for traces shown in (a). The line is a guide to the eye.

(A color version of this figure is available in the online journal.)

the sub-monolayer regime and by Acharyya et al. (2007) in the multilayer regime.

Next, we present the experimental evidence for molecular oxygen formation via combination of oxygen atoms. Figure 3 shows desorption of three O_2 isotopologues as a function of coverage after several simultaneous atomic ^{16}O and ^{18}O exposures (RF on) at 15 K. Comparing Figure 3 with molecularly adsorbed O_2 desorption shown in Figure 2, the most apparent difference is the desorption temperature. O_2 isotopologues desorb from the surface at a much higher temperature starting at about 57 ± 2 K. No such peak was observed in the desorption of O_2 after O_2 exposure at 20 K. We also monitored the mass-34 ($^{16}O^{18}O$) signal for evidence of prompt desorption during the deposition of ^{16}O and ^{18}O atoms. We did not detect the desorption of $^{16}O^{18}O$ molecules due to the Eley–Rideal formation mechanism during deposition. We conclude that these O_2 isotopologues form on the surface during the TPD phase when the surface temperature is raised. When resistive heating is applied to the sample during TPD, atomic oxygen species can overcome the diffusion energy barrier and become mobile. When two diffusing oxygen atoms meet, they form an O_2 molecule and immediately leave the surface. The conclusion that O_2 isotopologues form during TPD instead of during the exposure phase can also be backed by the unique way we conduct TPD at higher exposure temperatures (40 K, 50 K, and 60 K). After exposure, the surface is cooled down to 15 K before TPD (see the inset to Figure 7(a)). Assuming that the O_2 isotopologues have already formed during exposure, after cooling and during TPD, these molecules should desorb at about 30 K like the molecularly adsorbed O_2. Our experiments show no $^{16}O^{18}O$ desorption in the 30 K range.

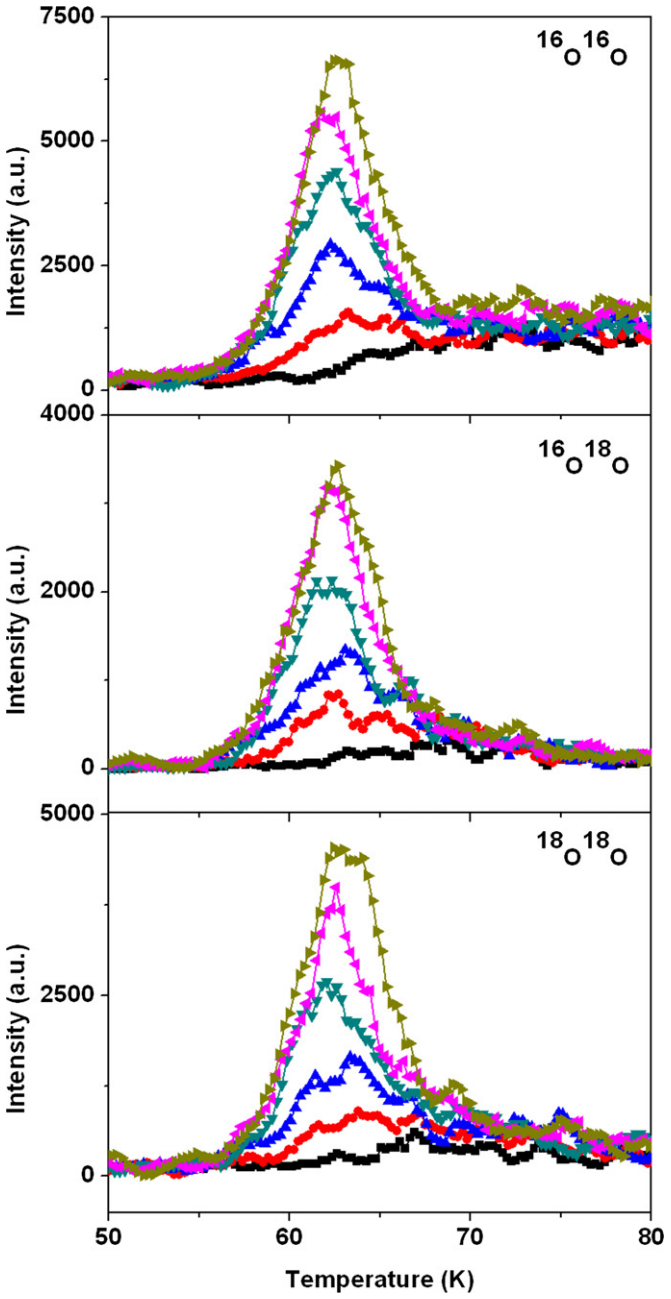

Figure 3. Desorption of molecular oxygen (top: $^{16}O_2$; middle: $^{16}O^{18}O$; bottom: $^{18}O_2$) formed by combination of O atoms after various exposures at 15 K. Peak stacking from bottom to top: 2 minute, 4 minute, 6 minute, 8 minute, 10 minute, and 12 minute exposures.

(A color version of this figure is available in the online journal.)

Following the formation of O_2 isotopologues, we present the mass spectra of O_3 isotopologues and isotopomers formed by the combination of O and O_2 on the surface. We could not obtain useful infrared spectra due to the low column density of O_3 molecules produced in our experiments. Figure 4 shows desorption of six kinds of O_3 molecules having four different masses after simultaneous atomic ^{16}O and ^{18}O exposures at 15 K. All O_3 molecules begin desorbing when the temperature

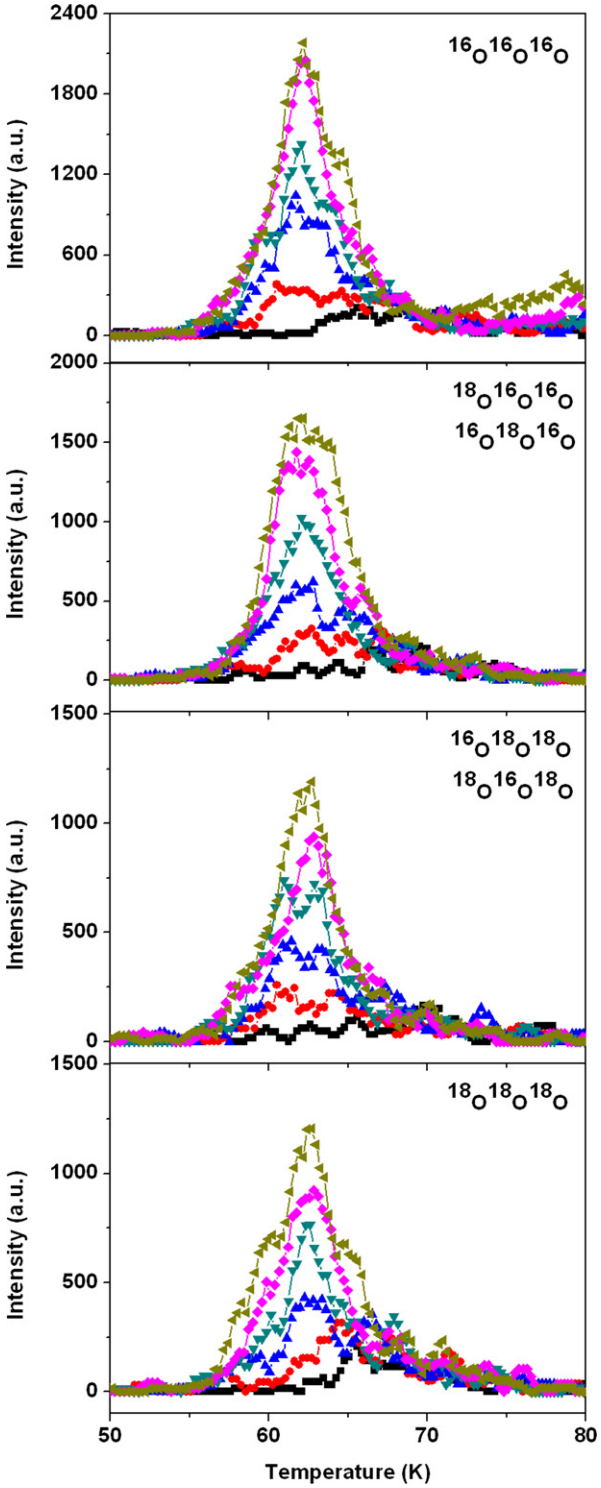

Figure 4. Desorption of ozone (from top to bottom: $^{16}O_3$, $^{18}O^{16}O_2$, $^{16}O^{18}O_2$, $^{18}O_3$) formed by combination of O and O_2 after various exposures at 15 K. Trace stacking from bottom to top: 2 minute, 4 minute, 6 minute, 8 minute, 10 minute, and 12 minute exposures.

(A color version of this figure is available in the online journal.)

reaches approximately 55 K. At about 73 K, all O_3 molecules have left the surface. Unlike the formation of O_2, where most molecules are believed to be formed during the TPD phase, we propose that most O_3 molecules are already formed before the TPD phase. In the case of O_2 formation, in the sub-monolayer coverage regime, as it is in our case, the reaction requires the diffusion of O atoms across the surface. However, at 15 K, O atoms do not have enough thermal energy to overcome the diffusion barrier (for an estimation of the diffusion barrier, see Section 3.2) and the tunneling effect is believed to be negligible. Therefore, O_2 can only form when the surface temperature is raised to the point where O atoms become mobile. However, in the case of O_3 formation, for sub-monolayer coverage and low surface temperature, even though O atoms are not diffusing, O_2 is still highly mobile. When a diffusing O_2 molecule meets an O atom, they can react and form an O_3 molecule. We acknowledge that not every O and O_2 encounter will form O_3. When an O_2 approaches an O atom, the angle between the O_2 velocity vector and its O=O bond axis has to fall within a certain range for the impact to be reactive. If the O atom fails to enter the cone of acceptance of the O_2 molecule, they will not react (Levine 2005). However, the details on the reaction dynamics are beyond the scope of this paper.

Finally, we show quantitatively that the formation of O_2 and O_3, as derived from our mass spectrometry experiments, depends on the sample temperature during exposure. At this point, it is necessary to point out the challenges of using mass spectrometry to analyze ozone formation due to ozone's poor stability and high reactivity. Three processes are taken into consideration. They are surface decomposition, gas phase (Fly path after desorbing from sample surface and before entering the QMS ionization chamber) decomposition, and electron-impact dissociation. First, Bennett & Kaiser (2005) suggest that ozone produced from 5 keV electron irradiation on O_2 ice is stable at 11 K. No decomposition or desorption is found from their infrared data. Second, Anderson & Mauersberger (1981) showed that ozone at room temperature in the gas phase has a half-life time of 12 hr. Therefore, we conclude that surface and gas-phase decomposition are negligible in our experiments. However, special care has to be taken for the electron-impact dissociation of O_2 and O_3. O_2 and O_3 molecules, when entering the ionization chamber of the mass spectrometer, undergo different ionization processes; some of the processes are listed below:

$$O_2 + e \rightarrow O^+ + O + 2e,\ O^+ + O_2 \rightarrow O_3^+ \quad (5)$$

$$O_3 + e \rightarrow O_3^+ + 2e \quad (6)$$

$$O_3 + e \rightarrow O_2^+ + O + 2e \quad (7)$$

$$O_3 + e \rightarrow O^+ + O_2 + 2e. \quad (8)$$

Therefore, it is clear that either O_2 or O_3 alone can produce O_2^+ and O_3^+ signals. As a result, one cannot determine the amount of O_2 and O_3 directly from O_2^+ and O_3^+ signals. To address the issue from Reactions (5), we look back at the molecularly adsorbed O_2 desorption experiments. Knowing no O_3 is present in these TPD runs, we find no O_3^+ signal appearing along with an O_2^+ signal. Hence, we conclude that the effect of Reactions (5) is negligible. Next, to address the issue of competing Reactions (6), (7), and (8), we conducted two control experiments. Experiment A is exposure of dissociated ^{16}O and ^{18}O beams (both beamlines RF on), whereas experiment B is exposure of atomic ^{16}O (RF on) and molecular $^{18}O_2$ (RF off). In experiment B, $^{16}O^{18}O$ molecules are not expected to form during TPD and the mass-34 signal is purely from electron-impact dissociation (Reaction (7)) of $^{16}O^{18}O_2$ molecules. On the other hand, in experiment A, the mass-34 TPD signal has two contributions, molecular $^{16}O^{18}O$ formation and electron-impact dissociation of $^{16}O^{18}O_2$. Comparing the mass-34 signal of these two control experiments, we conclude that the majority of the mass-34 signal is from

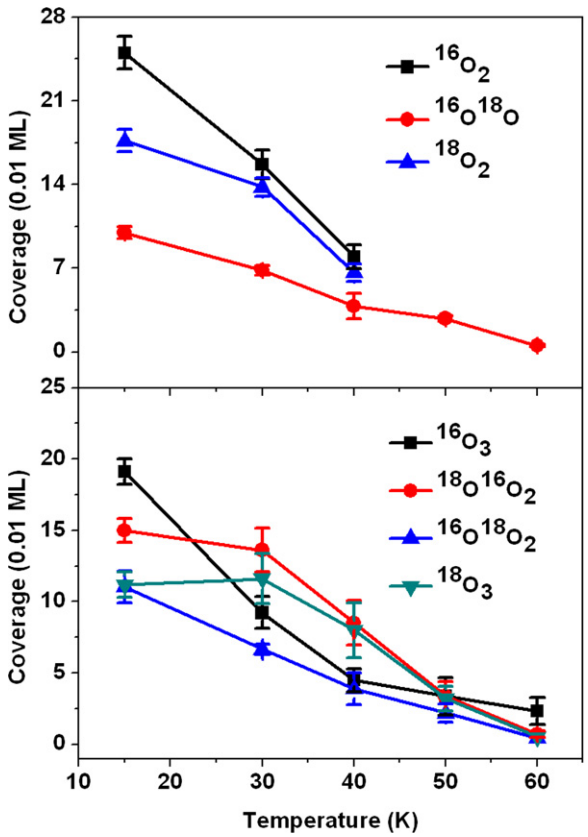

Figure 5. Desorption yield of O_2 and O_3 after 8 minutes of simultaneous ^{16}O and ^{18}O exposure as a function of exposure temperature.

(A color version of this figure is available in the online journal.)

$^{16}O^{18}O$ formation. However, the contribution of Reaction (7) is substantial and has to be evaluated quantitatively. We evaluate the relative weights of Reactions (6)–(8) using ionization cross-section data available from Newson et al. (1995) and Siegel (1982). Note that different isotopomers of O_3 make this evaluation even more complicated. Consider Reaction (7) of the molecule $^{16}O^{16}O^{18}O$ of C_s symmetry and $^{16}O^{18}O^{16}O$ of C_{2v} symmetry:

$$^{16}O^{16}O^{18}O + e \rightarrow {}^{16}O^{16}O^{+} + {}^{18}O + 2e \quad (7.1)$$

$$^{16}O^{16}O^{18}O + e \rightarrow {}^{16}O^{18}O^{+} + {}^{16}O + 2e \quad (7.2)$$

$$^{16}O^{18}O^{16}O + e \rightarrow {}^{16}O^{18}O^{+} + {}^{16}O + 2e. \quad (7.3)$$

One can see that the C_s molecule $^{16}O^{16}O^{18}O$ will affect the quantitative evaluation of both $^{16}O^{16}O$ through Reaction (7.1) and $^{16}O^{18}O$ through Reaction (7.2), whereas the C_{2v} molecule $^{16}O^{18}O^{16}O$ can only affect $^{16}O^{18}O$ through Reaction (7.3). Similarly, the C_s molecule $^{18}O^{18}O^{16}O$ will affect both $^{18}O^{18}O$ and $^{16}O^{18}O$, whereas the C_{2v} molecule $^{18}O^{16}O^{18}O$ can only affect $^{16}O^{18}O$. To account for this complication, we make the following two assumptions: (1) when an $^{16(18)}O_2$ molecule meets an $^{18(16)}O$ atom, formation of a C_s molecule or a C_{2v} molecule is equally probable. (2) For a C_s O_3 molecule, ionization through Reaction (7.1) or (7.2) is equally probable. Under these assumptions and using the available ionization cross-section data, we are able to estimate quantitatively the yield of all the O_2 and O_3 isotopologues and isotopomers.

In Figure 5, we show the desorption yield of O_2 and O_3 in units of monolayer coverage as a function of exposure temperature. The yield is derived from integration of a corresponding TPD peak and corrections from the above discussion have been applied. We emphasize that the yields shown here reflect the true amount of O_2 and O_3 species desorbed from the surface. The values are not necessarily proportional to the TPD peak areas due to the corrections. The yield of O_2 formation shows a decreasing trend with increasing exposure temperature. This trend can be explained by the temperature dependence of the sticking probability of both oxygen atoms and molecules on the surface. As exposure temperature increases, fewer atoms stick on the surface. Furthermore, atoms landing on "shallow" adsorption sites will be able to move if the exposure temperature is high enough (30 K and higher), resulting in O_2 formation and desorption before the TPD phase. Therefore, increasing the exposure temperature leads to a decreasing amount of O atoms to begin with and an increasing loss of O_2 molecules to be detected by the QMS during the TPD phase. The fact that the amount of $^{16}O^{18}O$ formed on the surface is smaller than the amount of either $^{16}O_2$ or $^{18}O_2$ can be explained by the non-perfect overlapping of the two atomic beams. Turning to the formation of O_3, it shows a similar behavior of decreasing yield with increasing exposure temperature. This is explained by the sticking probability of O_2 and its lifetime on the surface. After landing on the surface, an O_2 molecule will have a limited lifetime, before it desorbs and goes back to the gas phase, to diffuse on the surface and react with an O atom nearby to form O_3 and remain on the surface. As the exposure temperature (T) increases, the lifetime (τ) of O_2 decreases exponentially following the expression $\tau \sim \tau_0 \exp(E_{\rm des}/k_B T)$, where τ_0 is the characteristic time of vibration in the potential well ($\sim 10^{-12}$ s) and $E_{\rm des}$ is the desorption energy (see Section 3.2). Therefore, the probability of an O_2 molecule ending up incorporated into an O_3 within its lifetime will become less and less as the exposure temperature increases, and hence fewer and fewer O_3 molecules will form. In our experiments, we do not observe the significant isotope effect in the formation of O_3 isotopologues that was found by Sivaraman et al. (2011) in their experiments on 5 keV electron bombardment of an $^{16}O_2/^{18}O_2$ ice mixture. In their study, the heaviest isotope is six times more abundant than the lightest. However, their experiment differs from ours in the fact that the energetic electrons generate suprathermal O atoms in the O_2 ice matrix, and a fraction of the atoms so generated are electronically excited.

3.2. Rate Equation Simulation

In this subsection, we briefly show that our experimental data can be fitted to a rate equation model from which key energetic parameters can be obtained (Perets et al. 2007). First, we consider the experiment of O_2 desorption following the exposure of the sample to different doses of O_2. The number of O_2 molecules on the surface can by expressed as

$$\frac{dN(t)}{dt} = f(t) - \nu N(t) \exp\left(-\frac{E_{\rm des}}{k_B T(t)}\right), \quad (9)$$

where $N(t)$ is the number of O_2 molecules on the surface at time t. f is the incoming flux, which is the gain term. The second term is the desorption (loss) term, in which ν is the attempt frequency taken to be 10^{12} s^{-1}; $E_{\rm des}$ is the desorption energy; k_B is the Boltzmann constant; and T is the surface temperature. Time t starts at the onset of exposure (i.e., Equation (9) describes both the exposure phase and TPD phase). Since our surface is an amorphous thin film of silicate, the oxygen–silicate

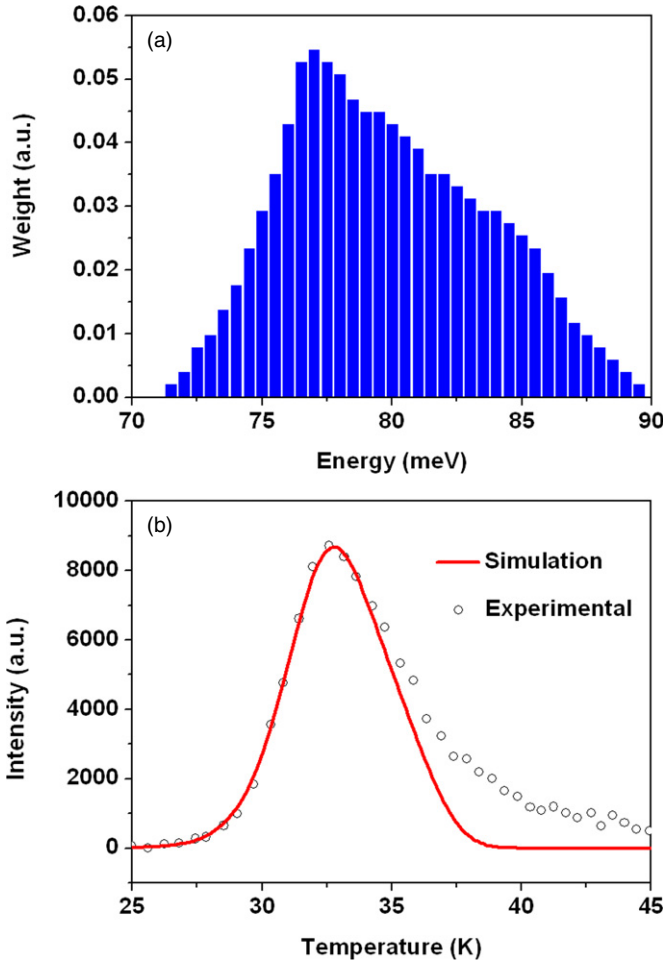

Figure 6. (a) Distribution of desorption energy of O_2 on amorphous silicate surface. (b) Desorption of O_2 after 6 minute exposure at 20 K. The solid curve is a simulated TPD experiment using the distribution of desorption energy shown in (a).

(A color version of this figure is available in the online journal.)

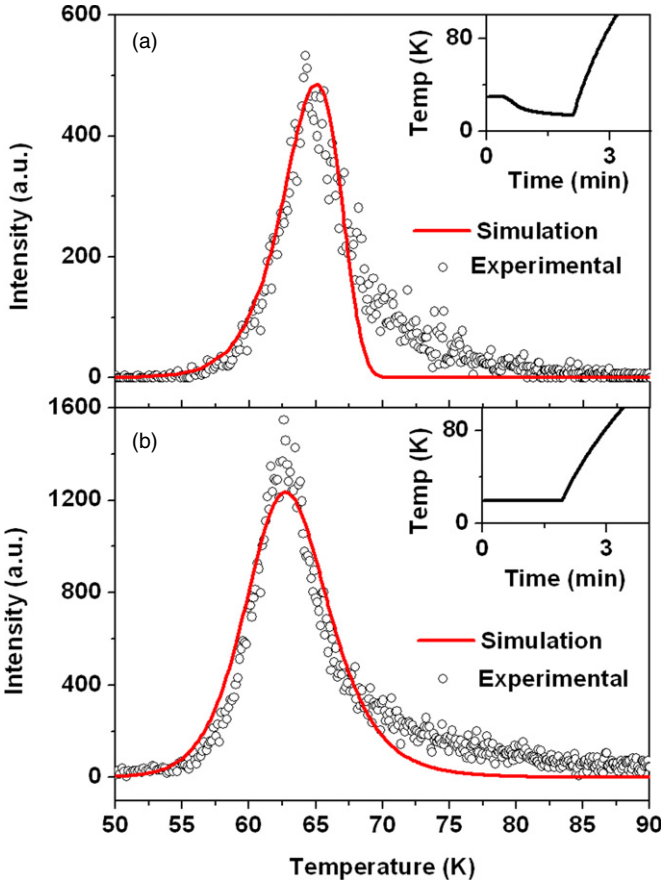

Figure 7. (a) Desorption of $^{18}O^{16}O_2$ after 8 minute simultaneous exposure of ^{16}O and ^{18}O at 30 K. The solid curve is a simulated TPD experiment using a 158 meV desorption energy. Inset: experimental temperature vs. time curve. (b) Desorption of $^{16}O^{18}O$ after 8 minutes of simultaneous exposure of ^{16}O and ^{18}O at 15 K. The solid curve is a simulated TPD experiment using a 154 meV desorption energy. Inset: experimental temperature vs. time curve.

(A color version of this figure is available in the online journal.)

potential energy surface is therefore not uniform. Similarly to our previous analysis of molecular hydrogen desorption from amorphous silicate film (He et al. 2011), we consider a range of desorption energy levels $E^i_{\rm des}$, with relative weights p_i, and Equation (9) becomes

$$\frac{dN_i(t)}{dt} = p_i f(t) - \nu N_i(t) \exp\left(-\frac{E^i_{\rm des}}{k_B T(t)}\right) \qquad (10)$$

$$N(t) = \sum\nolimits_{N_i}(t)$$

$$\sum\nolimits_{p_i} = 1.$$

By carefully adjusting $E^i_{\rm des}$ and p_i and fitting the simulated TPD curves with the experimental data, we are able to obtain the desorption energy distribution (see Figure 6(a)). The O_2 desorption energy ranges from 72 meV (835 K) to 90 meV (1045 K) and it peaks at 77 meV (890 K). Our result is in agreement with Acharyya et al. (2007), who found 912 ± 15 K for the energy of desorption of $^{16}O_2$ from an $^{16}O_2$ ice. In Figure 6(b), we show a simulated TPD curve using such a distribution and its corresponding experimental curve.

Next we move on to the desorption energy of O_3. Since most O_3 is formed isothermally before the TPD, the desorption of O_3 can be treated similarly to the case of desorption of O_2 shown above. In this case, to simplify the computation, we use Equation (9) with a single desorption energy value. From the fit we find this energy to be 158 ± 5 meV (1833 ± 60 K). The simulated TPD curve and its corresponding experimental data are shown in Figure 7(a). Because we used a single desorption energy value, the rate equation becomes the Polanyi–Wigner equation of first order and produces an asymmetrical desorption peak. It does not fully reproduce the width of the experimental curve due to the deviation from first-order desorption kinetics in the TPD experiment.

We now turn to the analysis of the formation of O_2. The rate equations describing O_2 formation are

$$\frac{dN_{\rm O}(t)}{dt} = -\nu N_{\rm O}(t) \exp\left(-\frac{E^{\rm O}_{\rm des}}{kT(t)}\right) - 2\frac{\nu}{S} N^2_{\rm O}(t) \exp\left(-\frac{E^{\rm O}_{\rm diff}}{k_B T(t)}\right) \qquad (11)$$

$$\frac{dN_{\rm O_2}(t)}{dt} = -\nu N_{\rm O_2}(t) \exp\left(-\frac{E^{\rm O_2}_{\rm des}}{k_B T(t)}\right) + \frac{\nu}{S} N^2_{\rm O}(t) \exp\left(-\frac{E^{\rm O}_{\rm diff}}{k_B T(t)}\right). \qquad (12)$$

Time t in these equations starts at the onset of the TPD phase (i.e., Equations (11) and (12) only describe the TPD phase). Initial values of N_O and N_{O_2} are taken to be the number of O atoms and O_2 molecules on the surface after exposure, but prior to TPD, and are estimated from the beam flux values with deductions from O_3 formation consumption. The first term on the right-hand side of Equation (11) is the term describing the desorption of oxygen atoms, where E^O_{des} is the desorption energy of O atoms. This term is considered to be negligible since, in the temperature range of interest, desorption of O atoms is not observed. The second term is the O_2 formation term, in which S is the adsorption site density on the surface. For our amorphous silicate sample, its value is 1.6×10^{15} cm^{-2}. This value is calculated from the O_2 adsorption/desorption experiment in which 10 minute exposure is considered to form 1 ML with the assumption of complete wetting. E^O_{diff} is the diffusion energy for O atoms. In Equation (12), the first term on the right-hand side is the desorption of O_2. The desorption energy is taken to be 77 meV determined from the above discussion. The second term is the formation of O_2 from combination of O atoms. We use Equations (11) and (12) to simulate the formation of O_2 and the result is shown in Figure 7(b). The atomic O diffusion energy extracted from this simulation is found to be 154 ± 3 meV (1785 ± 35 K). Due to the fact that the formation of O_2 is O diffusion limited, both experiment and simulation show second-order-like desorption kinetics, as seen from the symmetrical peaks.

4. ASTROPHYSICAL IMPLICATIONS

Despite its abundance, it has proven quite difficult to map the distribution of oxygen in the ISM. Jenkins (2009) re-analyzed archival data of the depletion of elements in the ISM. In accounting for the rate of depletion of oxygen, he concluded that it cannot be explained as due to integration into grains. For ISM environments from diffuse medium to molecular clouds, Whittet (2010) computed the amount of oxygen that is depleted from the gas phase into dust grains and oxygen-bearing ices. He showed that at the interface between diffuse and dense clouds, as much as 160 ppm of oxygen is not accounted for. Our experiments show that O_2 molecules have a similar binding energy on an amorphous silicate as they have on ice (∼80 meV or ∼930 K). Therefore, molecular oxygen uptake by bare dust grains (i.e., where there is a low A_v) can be ruled out since, at steady state and in ISM conditions, O_2 leaves the surface at around 16–18 K (Acharyya et al. 2007). However, oxygen atoms are more strongly bound and leave the surface as O_2 at a significant higher temperature (∼60 K), or remain on the surface and get hydrogenated to form OH. Ozone, in ISM environments, can be formed on silicate grains—in the absence of energetic sources—only when O_2 is present, which means the grain temperature should be less than 18 K. The binding energy of ozone on silicates is much higher than of O_2 on silicates and it could remain on the surface of the grain longer or at higher temperature. However, it is likely that O_3 is easily hydrogenated, in agreement that ozone has yet to be detected in the ISM. In any case, atomic oxygen can be stored on silicate surfaces at a considerably higher temperature than O_2. Can this be another significant reservoir of oxygen in low-A_v environments that has not been accounted for? Experiments and simulations of processes in ISM conditions will be needed to assess the weights of the competing processes of particle or photon desorption and reaction with H atoms.

5. SUMMARY

In experiments designed to probe oxygen interactions with grains in ISM environments using thermal energy beams of oxygen atoms impinging on a surface of an amorphous silicate film, we found that oxygen atoms are retained on the surface at much higher temperature (at least to 60 K) than molecular oxygen (∼18 K in steady-state conditions in ISM environments). The diffusion energy barrier (more precisely, a lower limit to it) of oxygen atoms on the surface of an amorphous silicate film was obtained.

This work is supported by the NSF, Astronomy & Astrophysics Division (grant No. 0908108), and by MIUR PRIN-08.

REFERENCES

Acharyya, K., Fuchs, G. W., Fraser, H. J., van Dishoeck, E. F., & Linnartz, H. 2007, A&A, 466, 1005
Anderson, S., & Mauersberger, K. 1981, Rev. Sci. Instrum., 52, 1025
Bennett, C. J., & Kaiser, R. I. 2005, ApJ, 635, 1362
Bergin, E. A., Kaufman, M. J., Melnick, G. J., Snell, R. L., & Howe, J. E. 2003, ApJ, 582, 830
Balucani, N., Stranges, D., Casavecchia, P., & Volpi, G. G. 2004, J. Chem. Phys., 120, 9571
Bergin, E. A., Melnick, G. J., Stauffer, J. R., et al. 2000, ApJ, 539, L129
Dohnalek, Z., Kim, J., Bondarchuk, O., White, J. M., & Kay, B. D. 2006, J. Phys. Chem. B, 110, 6229
Ehrenfreund, P., & Charnley, S. B. 2000, ARA&A, 38, 427
Ehrenfreund, P., & van Dishoeck, E. F. 1998, Adv. Space Res., 21, 15
Ennis, C. P., Bennett, C. J., & Kaiser, R. I. 2011, Phys. Chem. Chem. Phys., 13, 9469
Garrod, R. T., & Pauly, T. 2011, ApJ, 735, 18
Goldsmith, P. F., Melnick, G. J., Bergin, E. A., et al. 2000, ApJ, 539, L123
He, J., Frank, P., & Vidali, G. 2011, Phys. Chem. Chem. Phys., 13, 15803
Hincelin, U., Wakelam, V., Hersant, F., et al. 2011, A&A, 530, A61
Hollenbach, D., Kaufman, M. J., Bergin, E. A., & Melnick, G. J. 2009, ApJ, 690, 1497
Jenkins, E. B. 2009, ApJ, 700, 1299
Jing, D., He, J., Brucato, J., De Sio, A., Tozzetti, L., & Vidali, G. 2011, ApJ, 741, L9
King, D. A., & Wells, M. G. 1972, Surf. Sci., 29, 454
Kolasinski, K. W. 2008, Surface Science: Foundation of Catalysis and Nanoscience (New York: Wiley)
Levine, R. D. 2005, Molecular Reaction Dynamics (Cambridge: Cambridge Univ. Press)
Liseau, R., Larsson, B., Bergman, P., et al. 2010, A&A, 510, A98
Madzunkov, S. M., MacAskill, J. A., & Chutjian, A. 2010, ApJ, 712, 194
Meyer, D. M., Jura, M., & Cardelli, J. A. 1998, ApJ, 493, 222
Mokrane, H., Chaabouni, H., Accolla, M., et al. 2009, ApJ, 705, L195
Newson, K. A., Luc, S. M., Price, S. D., & Mason, N. J. 1995, Int. J. Mass pectrom. Ion Process., 148, 203
Pagani, L., Olofsson, A. O. H., Bergman, P., et al. 2003, A&A, 402, L77
Perets, H. B., Lederhendler, A., Biham, O., et al. 2007, ApJ, 661, L163
Raut, U., & Baragiola, R. A. 2011, ApJ, 737, L14
Romanzin, C., Ioppolo, S., Cuppen, H. M., van Dishoeck, E. F., & Linnartz, H. 2011, J. Chem. Phys., 134, 084504
Roser, J. E., Vidali, G., Manico, G., & Pirronello, V. 2001, ApJ, 555, L61
Siegel, M. W. 1982, Int. J. Mass Spectrom. Ion Process., 44, 19
Sivaraman, B., Jamieson, C. S., Mason, N. J., & Kaiser, R. I. 2007, ApJ, 669, 1414
Sivaraman, B., Mebel, A. M., Mason, N. J., Babikov, D., & Kaiser, R. I. 2011, Phys. Chem. Chem. Phys., 13, 421
Spaans, M., & van Dishoeck, E. F. 2001, ApJ, 548, L217
Whittet, D. C. B. 2010, ApJ, 710, 1009

The Astrophysical Journal, 780:113 (1pp), 2014 January 1 doi:10.1088/0004-637X/780/1/113

ERRATUM: "FORMATION OF MOLECULAR OXYGEN AND OZONE ON AMORPHOUS SILICATES" (2012, ApJ, 756, 98)

Dapeng Jing[1], Jiao He[1], John Robert Brucato[2], Gianfranco Vidali[1], Lorenzo Tozzetti[2], and Antonio De Sio[3]
[1] Physics Department, Syracuse University, Syracuse, NY 13244, USA; gvidali@syr.edu
[2] Osservatorio Astrofisico di Arcetri, INAF, I-50125 Florence, Italy
[3] Department of Physics and Astronomy, University of Florence, I-50125 Florence, Italy
Received 2013 October 9; published 2013 December 13

Online-only material: color figure

In the published article, from an examination of Figure 3 that represents the Temperature Programmed Desorption (TPD) peaks of atomic masses 32 ($^{16}O_2$), 34 ($^{16}O^{18}O$), and 36 ($^{18}O_2$) at about 63 K, we concluded that the reaction O+O→O_2, which was caused by atomic oxygen diffusion, was responsible for these peaks. This conclusion was based on two pieces of evidence: (1) the ozone fragmentation ratio calculated using the ionization cross-section data of Newson et al. (1995) and Siegel (1982) and (2) the comparison between control experiments A and B. After re-analyzing the data, we found a calculation mistake in the comparison of the control experiments. The ozone fragmentation ratio was calculated to the best of our knowledge and using the available literature; however, after carrying out new carefully designed experiments (He et al. 2014), we found out that the ionization cross-section data in Newson et al. (1995) and Siegel (1982) cannot be generalized to our system. Thus, we cannot quantify to which extent the TPD peaks mentioned above are due to ozone fragmentation in the ionizer of the detector. The following contents are also affected: (1) Figure 5, which is based on fragmentation ratio calculation, is not correct; a corrected Figure 5 is presented here. (2) The calculated atomic oxygen diffusion energy barrier value is not accurate and a new value based on new experiments and calculations is presented in He et al. (2014). All other results and conclusions are unaffected.

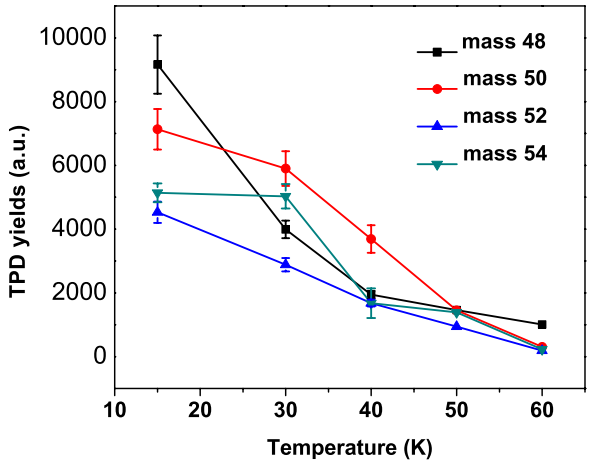

Figure 5. TPD QMS yields of atomic mass 48, 50, 52, and 54 after 8 minutes of simultaneous exposure of dissociated $^{16}O_2$ and $^{18}O_2$ beam at different temperatures. (A color version of this figure is available in the online journal.)

REFERENCES

He, J., et al. 2014, PCCP, submitted
Newson, K., Luc, S., Price, S., & Mason, N. 1995, IJMSI, 148, 203
Siegel, M. 1982, Int. J. Mass Spectrom. Ion Phys., 44, 19